Efficient Exciton Funneling in Cascaded PbS Quantum Dot Superstructures

Fan Xu,[†] Xin Ma,[†] Chelsea R. Haughn,[‡] Jamie Benavides,[†] Matthew F. Doty,[‡] and Sylvain G. Cloutier*[,†,§]

[†]Department of Electrical & Computer Engineering, University of Delaware, 140 Evans Hall, Newark, Delaware, United States, [‡]Department of Materials Science and Engineering, University of Delaware, 201 DuPont Hall, Newark, Delaware, United States, and [§]Département de Génie Électrique, École de Technologie Supérieure, 1100 Rue Notre-Dame Ouest, Montréal, Québec, Canada

ABSTRACT Benzenedithiol (BDT) and ethanedithiol (EDT) ligand-exchange treatments can be used to cross-link colloidal PbS quantum dots into nanocrystalline film structures with distinct optoelectronic properties. Such structures can provide a unique platform to study the energy transfer between layers of quantum dots with different sizes. In this report, efficient exciton funneling and recycling of surface state-bound excitons is observed in cascaded PbS quantum dot-based multilayered superstructures, where the excitons transfer from the larger band gap or *donor* layers to the smallest band gap or *acceptor* layers. In this system, both the BDT- and EDT-treated cascaded structures exhibit dramatically enhanced photoluminescence from the acceptor layers. As we show, the energy transfer mechanisms involved and their efficiencies are significantly different depending on the ligand-exchange treatment. In the future, we believe these efficient exciton recycling and funneling mechanisms could be used to improve significantly the photocurrent, charge-transport, and conversion efficiencies in low-cost nanocrystalline and hybrid solar cells and the emission efficiencies in hybrid light-emitting devices.

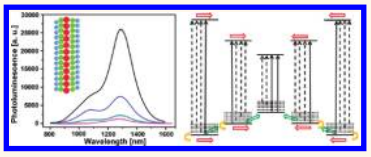

KEYWORDS: quantum dots · nanocrystalline solids · dithiol · Förster resonant energy transfer · exciton funneling · exciton recycling · photoluminescence

In recent years, short dithiolated cross-linking agents have been used to exchange the long capping groups around colloidal lead-chalcogenide nanocrystals, resulting in densely packed nanocrystalline solids with high conductivities.[1,2] Since then, some unique optoelectronic properties have been observed in these strongly coupled nanocrystalline solids, including superb multiple-exciton generation efficiencies,[3] efficient hot-electron injection,[4] and cold-exciton recycling,[5] thus pushing these self-assembled nanocrystalline structures to the forefront of optoelectronic materials and devices research.[6,7] However, one major limitation of such nanocrystalline solids is the significant loss of excitons to surface states. Indeed, it was previously shown that the photoluminescence (PL) efficiency of PbS quantum dots can easily drop from more than 50% in colloidal solutions to less than 1% in nanocrystalline solids.[8,9] One possible explanation is that photogenerated excitons efficiently transfer to nearby nonluminescent nanocrystals, where they recombine nonradiatively. Another possible explanation is that the formation of the nanocrystalline solid degrades surface passivation and increases the probability of nonradiative recombination in each nanoparticle. As such, developing efficient energy transport in nanocrystalline solids while reducing the loss to surface states is an important step toward the development of efficient nanocrystal-based optoelectronic devices.

The ability to carefully tune the band gap of colloidal nanocrystals combined with the controllable assembly of the nanocrystalline solids provides us with new ways to engineer the carrier conduction and to study energy transfer mechanisms.[1,10] For example, Förster resonance energy transfer (FRET) is a nonradiative energy transfer process resulting from dipole−dipole interactions.[11,12] This mechanism exists naturally in biological systems,[13] but it can also occur in artificially engineered structures with graded band gap.[5,14−16] For example, efficient FRET has been previously observed in various monodisperse and mixed colloidal nanocrystal assemblies, where excitons can flow along the gradient of decreasing band gaps.[5,17−20] In particular, efficient exciton funneling and recycling of trap state-bound excitons has been previously observed in CdTe nanocrystal assemblies with gradually changing band gaps, leading to significantly improved luminescence efficiencies.[5] However, the capping ligands used to passivate the nanocrystal surfaces also play a significant role in dictating the internanoparticle distance and the

* Address correspondence to sylvaing.cloutier@etsmtl.ca.

Received for review September 29, 2011 and accepted November 15, 2011.

Published online November 15, 2011
10.1021/nn203728t

density of surface states, and both of these properties strongly influence the FRET efficiency.[21−26]

In this report, we study exciton funneling in a cascaded film structure produced through layer-by-layer assembly of PbS nanocrystals with different sizes. We consider two different surfactants for the ligand-exchange process used to cross-link these superstructures: 1,2-ethanedithiol (EDT) and 1,3-benzenedithiol (BDT) molecules. We intuitively expect the EDT- and BDT-treated nanocrystalline solids will exhibit distinct optoelectronic properties because they have different backbone chain structures.[26−28] Indeed, the EDT molecule has a short C2 chain, while BDT is a conjugated dithiol molecule. Because of this difference, these dithiolated molecules provide a direct way to understand and control the energy transfer in self-assembled nanocrystalline films. In both the EDT- and BDT-treated cascaded superstructures, efficient exciton energy funneling can occur along the gradient of decreasing band gap, leading to dramatically improved photoluminescence in the acceptor layers. Using this mechanism, we demonstrate that the emission efficiency of a single monolayer of acceptor nanocrystals can show a 19-fold improvement when incorporated inside a BDT-treated cascaded superstructure, compared to a 13-fold enhancement inside an EDT-treated cascade. Controlled experiments including absorption, photoluminescence, and time-resolved photoluminescence spectroscopy measurements demonstrate that the recycling of trap state-bound excitons is primarily responsible for this significant efficiency enhancement.

RESULTS AND DISCUSSION

The lead-sulfosalt (PbS) nanocrystals are synthesized through a slightly modified version of the method pioneered by Hines and Scholes.[10] For the assembly of the nanocrystalline PbS solids, a carefully controlled layer-by-layer dip-coating method is employed using dithiol molecules (EDT or BDT) as cross-linking agents.[1] In this method, a clean glass substrate is first dipped into the diluted nanocrystal solution in hexane (<5 mg/mL) using a dip-coater and withdrawn at 200 mm/min. Once the film is dry, the substrate is immersed for 5 s in a 0.02 M solution of EDT or BDT and then quickly withdrawn. The careful control of this dip-coating process leads to the self-assembly of a nanocrystalline monolayer through each cycle.[1] In addition to replacing the electrically insulating oleic acid and cross-linking the nanocrystals, the dithiol treatment can also render the nanocrystals insoluble in common solvents. The TEM images in Figure 1 show ensembles of PbS nanocrystals capped with C18 oleic acid, BDT, and EDT. As shown in Figure 1(a), the oleic acid keeps the nanocrystals apart from each other with an average separation of ∼2.2 nm between nanocrystals, which is about twice the length of C18. As shown in Figure 1(b), treating the nanocrystals with BDT significantly reduces the interparticle spacing. Meanwhile, Figure 1(c) shows that the shorter and less bulky EDT linker brings the nanocrystals even closer to each other.

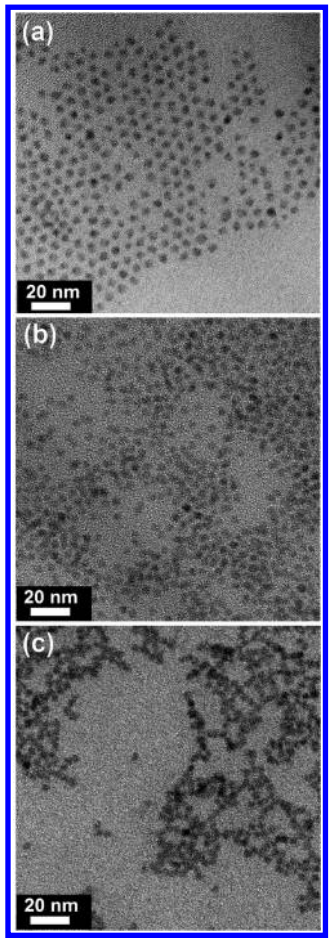

Figure 1. Transmission electron microscope images of PbS nanocrystals: (a) capped with C18 oleic acid; (b) cross-linked with BDT; (c) cross-linked with EDT.

Replacing long insulating ligands with cross-linking dithiols can dramatically enhance conductivity and energy transfer in nanocrystalline solids.[25−28] Here, Figure 2 compares the photoluminescence of oleic acid-, BDT-, and EDT-treated nanocrystalline solids produced under otherwise-identical conditions. As shown in Figure 2(a), the photoluminescence of the BDT-treated film exhibits a red shift of ∼35 nm, while the EDT-treated film's emission shows a much larger red shift of ∼71 nm compared to the pristine oleic acid-encapsulated nanocrystals. This red shift suggests efficient energy transfer from donor to acceptor across the inhomogeneous size distribution of nanocrystals. As expected from the smaller interparticle distance, this effect is much more pronounced in the EDT-treated film than in the BDT-treated film.[21]

The assembly of colloidal quantum dots into nanocrystalline solids also typically leads to a significant quenching of the photoluminescence. This quenching is attributed to fast exciton dissociation *via* tunneling to surface states, which results in Auger recombination

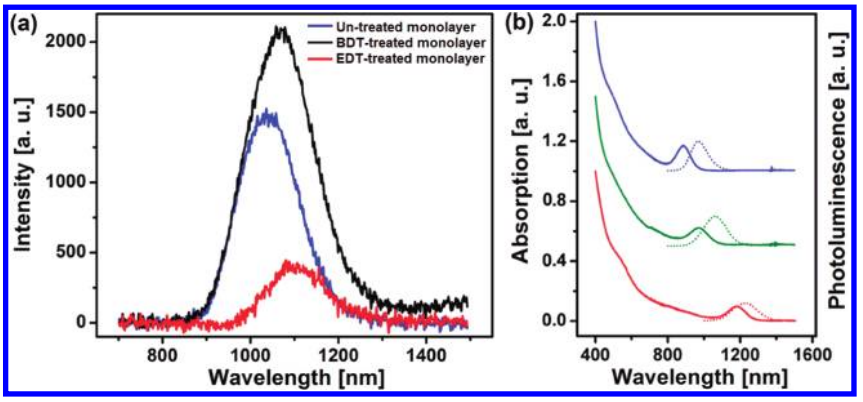

Figure 2. (a) Photoluminescence spectra of PbS quantum dot monolayers self-assembled on glass substrates and capped with oleic acid (blue), treated with BDT (black), and treated with EDT (red). (b) Absorbance and photoluminescence spectra for the three different PbS nanocrystal solutions later used to assemble our cascaded superstructures. In this article, the nanocrystals are identified by their emission peak in solution, namely, 980 nm (dotted blue), 1055 nm (dotted green), and 1240 nm (dotted red).

and capture of carriers by the nonradiative surface states.[8] While the photoluminescence from the EDT-treated nanocrystals is significantly quenched, the BDT-treated nanocrystals exhibit a moderate photoluminescence enhancement. To explain this effect, we measured the conductivity of the EDT and BDT cross-linked films using the charge extraction in linearly increasing voltage (CELIV) method.[8,29] The partial oxidization of dithiol-treated nanocrystals typically introduces p-type surface states into the nanocrystalline solids.[28−33] Using the CELIV method, the EDT-treated film displays a 40-fold higher conductivity (1.56×10^{-11} S/m) when compared with the BDT-treated film (3.91×10^{-13} S/m). This directly confirms the higher acceptor level in the EDT-treated structure compared with BDT. Thus, it can be reasonably speculated that in EDT-treated nanocrystalline solids, the fast exciton dissociation originates from short interparticle distance along with the higher density of surface states, which in turn dramatically quenches the photoluminescence. In contrast, the lower conductivity combined with a better surface passivation in the BDT-treated film suggests a lower impurity level, leading to a slightly improved photoluminescence.[8]

Cascaded superstructures are then produced using a layer-by-layer assembly of five monolayers of nanocrystals of three different sizes, with a stepwise-increasing size toward the center of the assembly. To achieve a cascaded structure favoring efficient energy transfer, the nanocrystal sizes are chosen so that there is a spectral overlap between the absorption of the acceptor nanocystals and the luminescence of the neighboring donor nanocrystals, such as shown in Figure 2(b).[11] From now on, we will identify the different nanocrystal sizes using their emission peak in solution (980, 1055, and 1240 nm), as shown in Figure 2(b).

We can first examine the energy transfer in a bilayered structure cross-linked with BDT. The structure consists of a monolayer of 1055 nm-emission

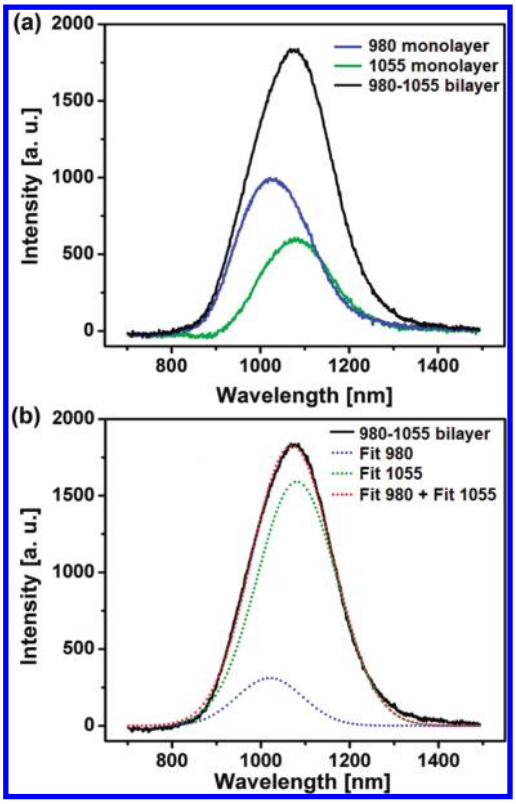

Figure 3. (a) Photoluminescence spectra for the 980 nm-emission nanocrystal monolayer (blue), 1055 nm-emission nanocrystal monolayer (green), and a 980-atop-1055 nm-emission bilayered structure cross-linked with BDT (black). (b) Photoluminescence spectra of a 980-atop-1055 nm-emission bilayered structure (black), and fitting curve with peak centered at the emission center of a single 980 nanocrystal monolayer (blue) and 1055 nanocrystal monolayer (green), as well as the sum of the fitting curves (red).

nanocrystals atop a monolayer of 980 nm-emission nanocrystals. As shown in Figure 3(a), the PL of this bilayered structure has a high degree of spectral overlap with the PL of a monolayer containing only 1055 nm-emission nanocrystals. The intensity of the PL emission is also dramatically enhanced. To clearly

resolve the enhancement of the acceptor (1055 nm-emission) nanocrystals' photoluminescence and quenching of the donor (980 nm-emission) nanocrystals' luminescence, we fit the bilayer's photoluminescence spectrum with two Gaussian curves centered at 980 nm (blue) and 1055 nm (green), as shown in Figure 3(b). Compared with the reference PL in Figure 3(a), the 1055 nm emission is enhanced by 165% in the bilayered film, while the 980 nm emission from the donor layer is quenched by 70%. Because the film of 1055 nanocrystals has the same density in the single- and bilayer structures, the PL enhancement indicates either an increased number of excitons or decreased nonradiative recombination in the 1055 nanocrystals. Inclusion of the 980 nanocrystals does not provide an obvious path to reduce nonradiative recombination in the 1055 nanocrystal film. However, inclusion of the 980 nanocrystals does provide a path for FRET or radiative transfer of excitons from the 980 to the 1055 nanocrystals.

In order to probe the energy transfer mechanism in the cascaded superstructure, we monitored the photoluminescence change through each step of the assembly, as shown in Figure 4(a). There, a single monolayer of acceptor nanocrystals (1240) is used as reference. When this layer of 1240 nanocrystals is deposited on top of a monolayer of 1055 nanocrystal donors, a moderate increase in acceptor emission is immediately observed, suggesting energy transfer. Then, when another layer of 1055 nanocrystal donors is deposited atop this structure, the emission from the 1240 nanocrystal acceptors increases suddenly by 5-fold compared with the single monolayer. Of course, the emission from the 1055 nanocrystals also increases considerably since there are now two such layers and one layer is on top at the incident surface. Finally, these three layers of 1055–1240–1055 nanocrystals can be sandwiched between two layers of 980 nanocrystal donors to form the five-layer 980–1055–1240–1055–980 nanocrystal cascade structure. There, the emission from the middle 1240 nanocrystal acceptor monolayer clearly dominates the emission from the other four layers with a dramatic 19-fold enhancement of the 1240 nm photoluminescence compared to a single monolayer of identical acceptor nanocrystals. These results clearly suggest a very efficient exciton transfer toward the middle layer of acceptor nanocrystals. However, this exciton funneling alone cannot explain the 19-fold photoluminescence enhancement of the cascaded structure. As we will show, the recycling of trap state-bound excitons in the cascaded structure appears to be the main process that contributes to this huge emission enhancement.

To conduct the experiments in a more controlled manner, we assembled five monolayers of 1240 nm-emission nanocrystals cross-linked with BDT and EDT for comparison with the five-layer cascaded superstructures. As shown in the absorption spectrum in Figure 4(b), the

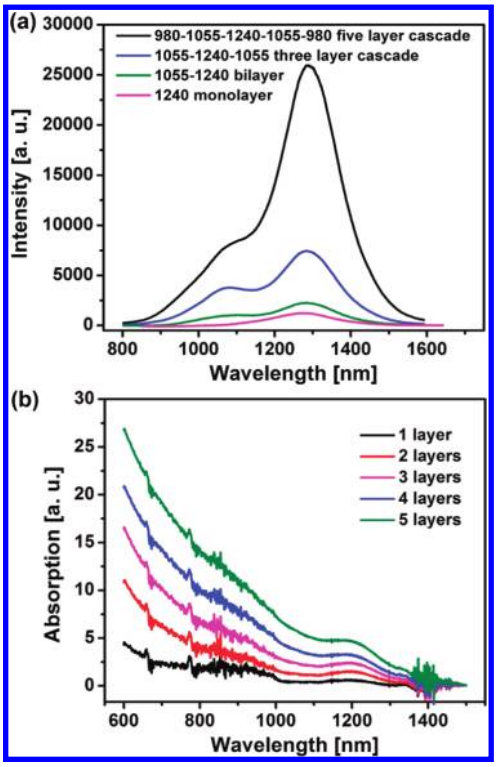

Figure 4. (a) Photoluminescence spectra for the 1240 nm-emission nanocrystal monolayer (pink), a 1240-atop-1055 nm-emission bilayered structure (green), 1055-atop-1240-atop-1055 nm-emission structure (blue), and the five-layer 980–1055–1240–1055–980 nm-emission cascaded nanostructure (black) all cross-linked with BDT. (b) Increase in absorption with monolayer-by-monolayer assembly of a PbS nanocrystalline solid linked with BDT.

absorption of the nanocrystalline solid increases steadily with the number of dip-coated nanocrystal monolayers, indicating that the number of quantum dots in each layer is comparable. However, the emission of the five-layer structure is significantly more than the 5-fold enhancement expected compared to the emission of a single layer, as shown in Figure 5(a). This increase in emission intensity suggests that there is less nonradiative recombination in the five-layer structure. This reduced nonradiative recombination can be attributed to FRET of excitons from surface state-bound nonradiative sites to other quantum dots where the excitons can radiatively recombine. In other words, the formation of the five-layer structure reduces the fraction of the exciton population that undergoes nonradiative recombination by depopulating the surface states and transferring those excitons to radiative recombination sites. As shown by the dotted line in Figure 5(a), the emission of the five-layer structure red-shifts in addition to increasing in intensity. This red shift further supports the conclusion that the luminescence intensity enhancement is due to FRET transfer. Transfer to lower energy states is energetically favored, and thus the transfer of excitons from surface-state nonradiative recombination sites to radiative quantum dot states at

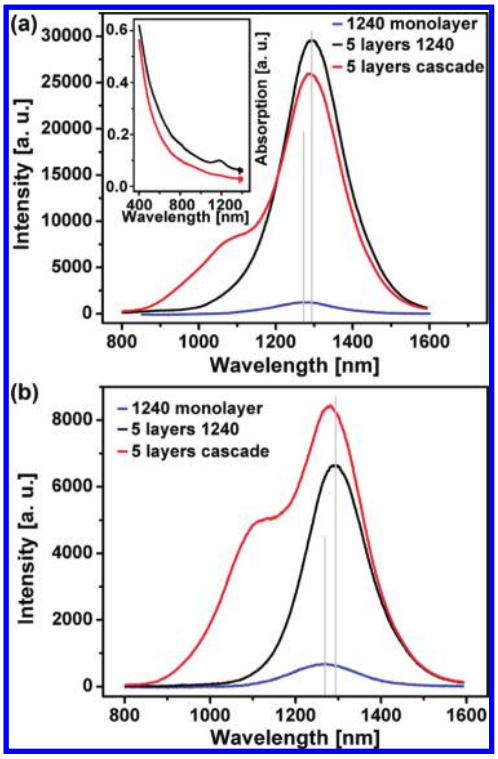

Figure 5. (a) Photoluminescence spectra of the BDT-treated five-layer cascaded superstructure (red), a five-layer stack of identical acceptor nanocrystals with 1240 nm emission (black), and a single monolayer of acceptor nanocrystals (blue). (b) Photoluminescence spectra of the EDT-treated five-layer cascaded superstructure (red), a five-layer stack of identical acceptor nanocrystals with 1240 nm emission (black), and a single monolayer of acceptor nanocrystals (blue).

lower energies is more common, as indicated by the red shift in photoluminescence.

The comparison between the photoluminescence and absorption spectra of the BDT-treated five-layer structures and the cascaded superstructure is shown in Figure 5(a). Although the integrated absorption of the assembly of five layers of 1240 nm-emission nanocrystals is 44% higher than the cascaded superstructure, the five layers' 1240 nm emission is only marginally higher than the 1240 nm monolayer's emission in the cascaded nanostructure. Furthermore, when integrating the photoluminescence emission over the entire spectra, the cascaded superstructure has a 5% higher intensity than that of the five-layer assembly of acceptor nanocrystals. This overall emission enhancement in the cascaded superstructure provides direct evidence for the efficient exciton recycling and transfer from the trap state-bound excitons to smaller band gap nanocrystals where they can now recombine radiatively.

As we have shown, the EDT treatment can result in strong energy transfer and leaves high densities of surface states in the nanocrystalline solids. This provides a convenient platform to study the trap state-bound exciton recycling in the EDT-treated cascaded superstructure. Figure 5(b) compares the photoluminescence from the cascaded superstructure and the five layers of acceptor nanocrystals cross-linked with EDT. The higher density of surface states and the strong interparticle coupling can lead to efficient recycling of trap state-bound excitons within this EDT-treated cascaded superstructure. Thus, the 1240 nm emission from the monolayer of acceptor nanocrystals within the cascaded nanostructures becomes stronger than the five-layer assembly of acceptor nanocrystals altogether, while the integrated emission intensity of the cascaded structure is still nearly twice that of the five layers of acceptor nanocrystals. Moreover, the emission peak also shows a small red shift in the five-layer assembly of acceptor nanocrystals, compared with the monolayer made of the same nanocrystals. Again, this suggests that the exciton funneling and trap state-bound exciton recycling can also occur across the size distribution of the nanocrystals toward the larger quantum dots. However, it must be pointed out that the high density of surface states present in the EDT-treated samples can still quench the emission after the excitons transfer to the larger nanocrystals. As a result, the emission enhancement factor observed for the EDT-treated nanocrystals is only roughly 66% of the enhancement factor measured for the BDT-treated cascade structure.

Based on these measurements, Figure 6 illustrates the dominant transfer and recombination pathways for excitons in the EDT- and BDT-treated cascade structures. Upon excitation, a great fraction of the carriers can be captured by the surface states,[33] especially in the EDT-treated structures where the density of trapping centers is high. Those trap state-bound excitons can either resonantly transfer to neighboring smaller band gap nanocrystals or recombine nonradiatively. Both the BDT- and EDT-treated cascade structures can recycle the trap state-bound excitons into smaller band gap nanocrystal neighbors. However, the BDT treatment passivates the nanocrystal surfaces better and leads to higher emission efficiency, while the EDT treatment leads to more trap state-bound exciton recycling owing to a shorter interparticle distance and larger densities of trap states.

To better understand this exciton transfer, we can also examine the time-resolved photoluminescence of PbS nanocrystals in the bilayered donor–acceptor structure. For the results shown in Figure 7, smaller nanocrystals with emission centered at 950 nm are used as donors, while nanocrystals with emission centered at 1020 nm are used as acceptors. While the untreated oleic acid-encapsulated donor nanocrystals show a long exciton lifetime of 278 ns, the dithiol treatment significantly lowers the exciton lifetime. Indeed, the BDT treatment yields an exciton lifetime of $\tau_d = 77$ ns in the donor-only monolayer compared to $\tau_{da} = 40$ ns in a donor–acceptor bilayered structure. Meanwhile, the exciton lifetime in the EDT-treated films is much shorter owing to the smaller interparticle

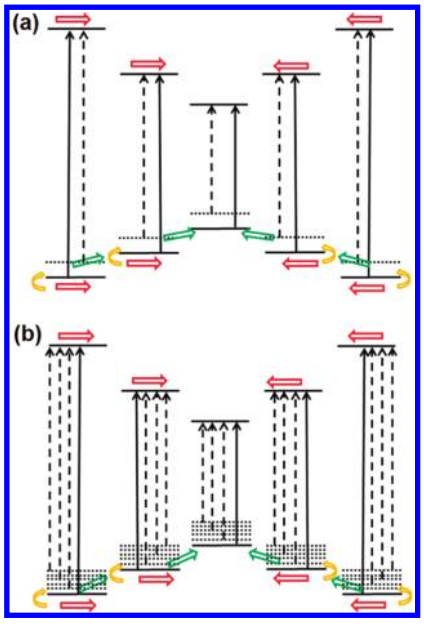

Figure 6. Schematic band alignment of the cascaded superstructures (a) cross-linked with BDT and (b) cross-linked with EDT. The solid black lines represent the conduction and valence band of the nanocrystals, and the dotted lines represent the trap states' energy levels. The solid arrows indicate the radiative recombination and dotted arrows indicate the nonradiative recombination. The red arrows show the direction of exciton funneling, the gold arrows indicate the relaxation of excitons to trap states, and the green arrows indicate the recycling of trap state-bound excitons. The free excitons can easily bind to trap states, especially in the EDT-treated structures where the density of trap states is higher. However, these trap state-bound excitons can be resonantly transferred to the smaller band gap nanocrystal neighbors (exciton recycling process).

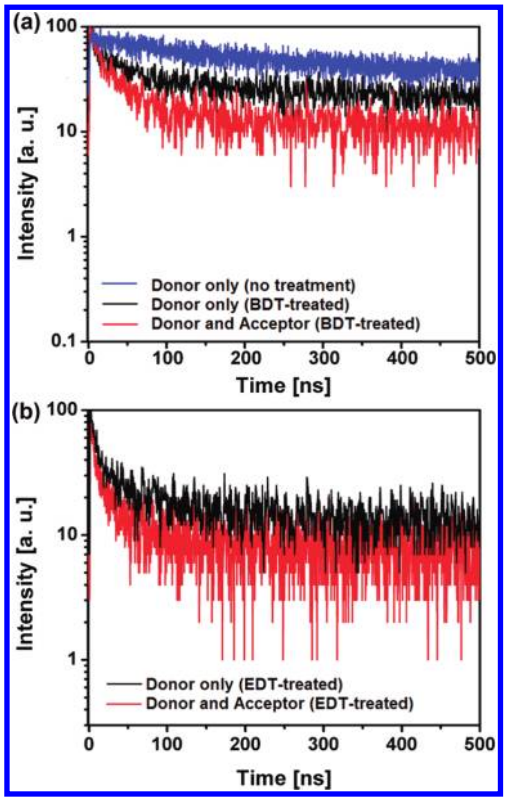

Figure 7. Time-resolved photoluminescence of PbS nanocrystals detected at the donor peak wavelength of 950 nm. (a) Donor nanocrystals capped with oleic acid (blue), donor nanocrystals cross-linked with BDT (black), and BDT-treated donor–acceptor bilayered structure (red). (b) Donor nanocrystals cross-linked with EDT (black) and EDT-treated donor–acceptor bilayered structure (red).

distance and the faster nonradiative recombination originating from surface states, which significantly reduces the exciton lifetime. Indeed, the exciton lifetime is τ_d = 57 ns for the donor-only EDT-treated film and only τ_{da} = 27 ns in the EDT-treated donor–acceptor bilayered structure. The exciton decay lifetime measured here is somewhat larger than the value reported previously,[21] presumably because this earlier study deals with more closely packed and thicker nanocrystalline solids made by drop-casting. We anticipate that time-resolved photoluminescence measurements of the emission from the acceptor nanocrystals would reveal enhanced lifetime and support the conclusion that FRET transfer can funnel excitons from nonradiative states to radiative states at lower energy. Unfortunately the wavelength sensitivity of conventional silicon avalanche photodiode prevents us from undertaking these measurements.

The FRET efficiency estimated using $\eta = 1 - (\tau_d/\tau_{da})$ provides a rough estimate of the quenching of the donor emission and the corresponding enhancement in acceptor emission.[18] The FRET depends strongly on the interparticle distance as $(R_F/R)^6$, where R_F is the Förster radius and R is the interparticle distance.[34–37] Since the EDT is slightly shorter than BDT, the FRET efficiency measures 53% in the EDT-treated bilayer, compared with 48% in the BDT-treated structure. On the basis of these results, if we assume a ~50% FRET efficiency between each of the five cascaded layers, the maximum emission enhancement in the acceptor monolayer in the center of the cascaded structure would be only 150% (3-fold). Thus, FRET of free excitons does not suffice to explain the 19-fold increase observed in the BDT-treated cascade and the 13-fold enhancement in the EDT-treated cascade. Recycling of trap state-bound excitons explains the large emission enhancement observed.

CONCLUSION

We provide clear evidence that excitons can be funneled through the decreasing band gap of a multilayered cascaded superstructure fabricated using monolayers of nanocrystals with different sizes. Most importantly, we demonstrate that the luminescence of nanocrystalline solids can be dramatically improved through the recycling of trap state-bound excitons in dithiol-treated cascaded superstructures. These results establish that both the BDT- and EDT-treated cascades exhibit efficient exciton funneling. Shorter interparticle separation and a high density of

surface states in the EDT-treated structures result in stronger trap state-bound exciton recycling. The BDT treatment leads to much higher emission efficiencies because of better surface passivation. We observe that the emission of a single monolayer of acceptor nanocrystals is enhanced 19-fold when embedded in a five-layer BDT-treated cascade structure and 13-fold in a five-layer EDT-treated cascade. In the future, these cascaded nanocrystal superstructures could be used to provide highly efficient nanocrystal-based near-infrared light emitting devices. Moreover, the ability to control the exciton energy flow and the recycling of trap state-bound excitons also opens exciting new possibilities to enhance the photocurrent and carrier transport in low-cost nanocrystalline and hybrid solar cell structures.

METHODS

Chemicals. Lead oxide (99.99%, Aldrich), hexamethyldisilathiane (Fluka), oleic acid (90%, Aldrich), 1-octadecene (90%, Aldrich), 1,2 ethanedithiol (>98%, Fluka), 1,3 benzenedithiol (99%, Aldrich), and anhydrous acetonitrile (99.8%, Sigma Aldrich) were used.

Synthesis. Lead-sulfosalt nanocrystals are synthesized through a slightly modified version of the method pioneered by Hines *et al.*[10] For the synthesis, lead oxide (0.45 g), octadecene (10 g), and oleic acid (1.34 g) are added to a three-neck flask. The mixture is then heated and kept at 80 °C for two hours under vigorous stirring under vacuum to degas and dissolve the mixture. The temperature is then kept at 110 °C under nitrogen flow for 30 min. Subsequently, a solution made of 210 μL of hexamethyldisilathiane diluted in 4 mL of octadecene is quickly injected into the reaction flask, and the heating was immediately removed. The reaction solution was allowed to cool to room temperature slowly. Finally, the colloidal PbS quantum dots are collected by quick injection of the reaction solution into an excess amount of acetone (with ratio ~1:4) for centrifugation. The precipitates are dried under vacuum and redispersed in hexane. To ensure adequate removal of the reaction solvents, precipitation and redispersion are repeated several times, and the quantum dot solution is finally filtered with 0.2 μm polytetreafluoroethylene filters. The size of the nanorystals can be controlled by adjusting the amount of oleic acid in the reaction. Higher oleic acid concentration leads to larger nanocrystals.

Preparation of Nanocrystalline (NC) Solids Using Layer-by-Layer Dip-Coating. The entire process was conducted in a fume-hood under ambient atmosphere. Substrates were dipped by dip-coater into a diluted solution of PbS NCs in hexane (<5 mg/mL) and slowly removed from the solution at a speed of 200 mm/min. Once dry, the substrate was dipped into a beaker containing 0.02 M EDT (or BDT) in anhydrous acetonitrile for 5 s and removed. Once the substrate is dry, a second NC layer can be deposited on top.

Characterization. TEM images were obtained using a JEM 2010F instrument at an acceleration voltage of 200 keV. Photoluminescence measurements were performed at room temperature using a Jobin-Yvon iHR320 triple-grating spectrometer equipped with a Symphony thermoelectric-cooled CCD array. For photoluminescence excitation, we used a 250 mW frequency-stabilized TORUS (Laser-Quantum) laser operating at 532 nm. For time-resolved photoluminescence measurements, we used the Mira-900 fs pulsed laser runs at the repetition rate of 151 kHz, and the excitation wavelength was 780 nm. The excitation wavelength was filtered from the PL with an 800 nm long pass filter and a ND1 neutral density filter. The time-resolved PL was detected at the donor peak wavelength of 950 nm using a Perkin-Elmer avalanche photodiode with a PicoHarp time correlated single photon counting system. The spectral bandwidth was 25 nm. The time-resolved PL data were fitted using FluoFit data analysis software from PicoQuant.

Acknowledgment. We thank Sangcheol Kim for the absorption measurements. This work was supported by the DARPA COMPASS program through a grant from DOI NBC (N11AP20031) and by the AFOSR (FA9550-10-1-0363).

REFERENCES AND NOTES

1. Luther, J. M.; Law, M.; Song, Q.; Perkins, C. L.; Beard, M. C.; Nozik, A. J. Structural, Optical, and Electrical Properties of Self-Assembled Films of PbSe Nanocrystals Treated with 1,2-Ethanedithiol. *ACS Nano* **2008**, *2*, 271–280.
2. Moody, I. S.; Stonas, A. R.; Lonergan, M. C. PbS Nanocrystals Functionalized with a Short Ionic, Dithiol Ligand. *J. Phys. Chem. C* **2008**, *112*, 19383–19389.
3. Ellongson, R. J.; Beard, M. C.; Johnson, J. C.; Yu, P.; Micic, O. I.; Nozik, A. J.; Shabaev, A.; Efros, A. L. Highly Efficient Mutiple Exciton Generation in Colloial PbSe and PbS Quantum Dots. *Nano Lett.* **2005**, *5*, 865–871.
4. Tisdale, W. A.; Williams, K. J.; Timp, B. A.; Norris, D. J.; Aydil, E. S.; Zhu, X. Y. Hot-Electron Transfer from Semiconductor Nanocrystals. *Science* **2010**, *18*, 1543–1547.
5. Franzl, T.; Klar, T. A.; Schietinger, S.; Rogach, A. L.; Feldmann, J. Exciton Recycling in Graded Gap Nanocrystal Structure. *Nano Lett.* **2004**, *9*, 1599–1603.
6. Sukhovatkin, V.; Hinds, S.; Brzozowski, L.; Sargent, E. H. Colloidal Quantum-Dot Photodetectors Exploiting Multiexciton Generation. *Science* **2009**, *324*, 1542–1544.
7. Pattantyus-Abraham, A. G.; Kramer, I. J.; Barkhouse, A. R.; Wang, X.; Kanstantatos, G.; Debnath, R.; Levina, L.; Raabe, I.; Nazeeruddin, M. K.; Gratzel, M.; *et al.* Depleted-Heterojunction QD Solar Cells. *ACS Nano* **2010**, *4*, 3374–3380.
8. Aaron, D.; Barkhouse, R.; Pattantyus-Abraham, A. G.; Levina, L.; Sargent, E. H. Thiols Passivate Recombination Centers in Colloidal Quantum Dots Leading to Enhanced Photovoltaic Device Efficiency. *ACS Nano* **2008**, *2*, 2356–2362.
9. Chang, T. F.; Maria, A.; Cyr, P. W.; Sukhovatkin, V.; Levina, L.; Sargent, E. H. High Near-Infrared Photoluminescence Quantum Efficiency from PbS Nanocrystals in Polymer Films. *Synth. Met.* **2004**, *148*, 257–261.
10. Hines, M. A.; Scholes, G. A. Colloidal PbS Nanocrystals with Size-Tunable Near-Infrared Emision: Observation of Post-Synthesis Self-Narrowing of the Particle Size Distribution. *Adv. Mater.* **2003**, *15*, 1844–1849.
11. Scholes, G. D. Long-Rang Resonance Energy Transfer in Molecular Systems. *Annu. Rev. Phys. Chem.* **2003**, *54*, 57–87.
12. Förster, T. Zwischenmolekulare Energiewanderung und Fluoreszenz. *Ann. Phys.* **1948**, *6*, 55–75.
13. Kühlbrandt, W. Many Wheels Make Light Work. *Nature* **1995**, *374*, 497–498.
14. Giménez, S.; Rogach, A. L; Lutich, A. A.; Gross, D.; Poeschi, A.; Susha, A. S.; Mora-Seró, I.; Lana-Villarreal, T.; Bisquert, J. Energy Transfer versus Charge Separation in Hybrid Systems of Semiconductor Quantum Dots and Ru-Dyes as Potential Co-Sensitizers of TiO_2-Based Solar Cells. *J. Appl. Phys.* **2011**, *110*, 014314.
15. Koposov, A. Y.; Cardolaccia, T.; Albert, V.; Badaeva, E.; Kilina, S.; Meyer, T. J.; Tretiak, S.; Sykora, M. Formation of Assemblies Comprising Ru-Polypyridine Complexes and CdSe Nanocrystals Studied by ATR-FTIR Spectroscopy and DFT Modeling. *Langmuir* **2011**, *27*, 8377–8383.
16. Mora-Seró, I.; Gross, D.; Mittereder, T.; Lutich, A.; Susha., A. S.; Dittrich, T.; Belarid, A.; Caballero, R.; Langa, F.;

Bisquert, J.; *et al.* Nanoscale Interaction Between CdSe and CdTe Nanocrystals and Molecular Dyes Forserting or Hindering Directional Charge Separation. *Small* **2010**, *6*, 221–225.
17. Crooker, S. A.; Hollingsworth, J. A.; Tretiak, S.; Klimov, V. I. Spectrally Resolved Dynamics of Energy Transfer in Quantum Dot Assemblies: Towards Engineered Energy Flows in Artificial Materials. *Phys. Rev. Lett.* **2002**, *89*, 186802.
18. Bose, R.; Mcmillan, J. F.; Gao, J.; Rickey, K. M.; Chen, C. J.; Talapin, D. V.; Murray, C. B.; Wong, C. W. Temperature-Tuning of Near-Infrared Monodisperse Quantum Dot Solids at 1.5 μm for Controllable Förster Energy Transfer. *Nano Lett.* **2008**, *8*, 2006–2011.
19. Lü, W.; Kamiya, I.; Ichida, M.; Ando, H. Temperature Dependence of Electronic Energy Transfer in PbS Quantum Dot Films. *Appl. Phys. Lett.* **2009**, *95*, 083102.
20. Lunz, M.; Bradley, A. L.; Gerard, V. A.; Byrne, S. J.; Gun'ko, Y. K.; Lesnyak, V.; Gaponik, N. Concentration Dependence of Förster Resonant Energy Transfer between Donor and Acceptor Nanocrystal Quantum Dot Layers: Effect of Donor-Donor Interactions. *Phys. Rev. B* **2011**, *83*, 115423.
21. Choi, J. J.; Luria, J.; Hyun, B. R.; Bartnik, A. C.; Sun, L.; Lim, Y. F.; Marohn, J. A.; Wise, F. W; Hanrath, T. Photogenerated Exciton Dissociation in Highly Coupled Lead Salt Nanocrystal Assemblies. *Nano Lett.* **2010**, *10*, 1805–1811.
22. Hinds, S.; Levina, L.; Klem, E. J. D.; Konstantatos, G.; Sukhovatkin, V.; Sargent, E. H. Smooth-Morphology Ultrasensitive Solution-Processed Photodetectors. *Adv. Mater.* **2008**, *20*, 1–5.
23. Koleiat, G. I.; Levina, L.; Shukla, H.; Myrskog, S. H.; Hinds, S.; Pattantyus-Abraham, A. G.; Sargent, E. H. Efficient, Stable Infrared Photovoltaics Based on Solution Cast Colloidal Quantum Dots. *ACS Nano* **2008**, *2*, 833–840.
24. Lingley, Z.; Lu, S.; Madhukar, A. A High Quantum Efficiency Preserving Approach to Ligand Exchange on Lead Sulfide Quantum Dots and Interdot Resonant Energy Transfer. *Nano Lett.* **2011**, *11*, 2887–2891.
25. Zarghami, M. H.; Liu, Y.; Gibbs, M.; Gebremichael, E.; Webster, C.; Law, M. p-Type PbSe and PbS Quantum Dot Solids Prepared with Short-Chain Acids and Diacids. *ACS Nano* **2010**, *4*, 2475–2485.
26. Liu, Y.; Gibbs, M.; Puthussery, J.; Gaik, S.; Ihly, R.; Hillhouse, H. W.; Law, M. Dependence of Carrier Mobility on Nanocrystal Size and Ligand Length in PbSe Nanocrystal Solids. *Nano Lett.* **2010**, *10*, 1960–1969.
27. Kim, Y.; Pietsch, T.; Erbe, A.; Belzig, W.; Scheer, E. Benzenedithiol: A Broad-Range Single-Channel Molecular Conductor. *Nano Lett.* **2011**, *11*, 3734–3738.
28. Sarasqueta, G.; Choudhury, K. R.; So, F. Effect of Solvent Treatment on Solution-Processed Colloidal PbSe Nanocrystal Infrared Photodetectors. *Chem. Mater.* **2010**, *22*, 3496–3501.
29. Johnston, K. W.; Pattantyus-Abraham, A. G.; Clifford, J. P.; Myrskog, S. H.; Hoogland, S.; Shukla, H.; Klem, E. J. D.; Levina, L.; Sargent, E. H. Efficient Schottky-Quantum-Dot Photovoltaics: The Roles of Depletion Drift, and Diffusion. *Appl. Phys. Lett.* **2008**, *92*, 122111.
30. Ma, W.; Lutherm, J. M.; Zheng, H.; Wu, Y.; Alivisatos, A. P. Photovoltaic Devices Employing Ternary PbS_xSe_{1-x} Nanocrystals. *Nano Lett.* **2009**, *9*, 1699–1703.
31. Norris, D. J.; Efros, A. L.; Erwin, S. C. Doped Nanocrystals. *Science* **2008**, *319*, 1776–1779.
32. Beard, M. C.; Midgett, A. G.; Law, M.; Semonin, O. E.; Ellingson, R. J.; Nozik, A. J. Multiple Exciton Generation for a Series of Chemically Treated PbSe Nanocrystal Films. *Nano Lett.* **2009**, *9*, 836–845.
33. Klem, E. J. D.; Shukla, H.; Hinds, S.; MacNeil, D. D.; Levina, L.; Sargent, E. H. Impact of Dithiol Treatment and Air Annealing on the Conductivity, Mobility, and Hole Density in PbS Colloidal Quantum Dot Solids. *Appl. Phys. Lett.* **2008**, *92*, 212105.
34. Kapitonov, A. V.; Stupak, A. P.; Gaponenko, S. V.; Petrov, E. P.; Rogach, A. L.; Eychmüller, A. L. Luminescence Properties of Thiol-Stabilized CdTe Nanocrystals. *J. Phys. Chem. B* **1999**, *103*, 10109–10113.
35. Wu, Z.; Mi, Z.; Bhattacharya, P.; Zhu, T.; Xu, J. Enhanced Spontaneous Emission at 1.55 μm from Colloidal PbSe Quantum Dots in a Si Photonic Crystal Microcavity. *Appl. Phys. Lett.* **2007**, *90*, 171105.
36. Fushman, I.; Englund, D.; Vuckovic, J. Coupling of PbS Quantum Dots to Photonic Crystal Cavities at Room Temperature. *Appl. Phys. Lett.* **2005**, *87*, 241102.
37. Kramer, I. J.; Levina, L.; Debnath, R.; Zhitomirsky, D.; Sargent, E. H. Solar Cells Using Quantum Funnels. *Nano Lett.* **2011**, *11*, 3701–3706.